Geophysical Research Letters

RESEARCH LETTER
10.1029/2024GL112266

Mercury's Tidal Love Number h_2 From Co-Registration of MLA Profiles

Haifeng Xiao[1], Alexander Stark[2], Gregor Steinbrügge[3], Arthur Briaud[4], Luisa M. Lara[1], and Pedro J. Gutiérrez[1]

[1]Instituto de Astrofísica de Andalucía (IAA-CSIC), Granada, Spain, [2]Institute of Planetary Research, German Aerospace Center (DLR), Berlin, Germany, [3]Jet Propulsion Laboratory, California Institute of Technology, Pasadena, CA, USA, [4]Institute of Geodesy and Geoinformation Science, Technische Universität Berlin, Berlin, Germany

Key Points:

- We show the feasibility and merits of co-registering Mercury Laser Altimeter profiles in detecting the tidal deformation of Mercury
- The measured tidal Love number h_2 is 0.92±0.58 (3-σ), compatible with existing modelings
- The central value of the measured h_2 would favor a small to medium-sized solid inner core

Supporting Information:

Supporting Information may be found in the online version of this article.

Correspondence to:

H. Xiao,
hxiao@iaa.es

Citation:

Xiao, H., Stark, A., Steinbrügge, G., Briaud, A., Lara, L. M., & Gutiérrez, P. J. (2025). Mercury's tidal Love number h_2 from co-registration of MLA profiles. *Geophysical Research Letters*, *52*, e2024GL112266. https://doi.org/10.1029/2024GL112266

Received 30 AUG 2024
Accepted 26 JAN 2025

Author Contributions:

Conceptualization: Haifeng Xiao, Alexander Stark, Luisa M. Lara, Pedro J. Gutiérrez
Data curation: Haifeng Xiao
Formal analysis: Haifeng Xiao, Alexander Stark, Gregor Steinbrügge, Arthur Briaud, Luisa M. Lara, Pedro J. Gutiérrez
Funding acquisition: Luisa M. Lara, Pedro J. Gutiérrez
Investigation: Haifeng Xiao, Alexander Stark, Gregor Steinbrügge, Arthur Briaud, Luisa M. Lara, Pedro J. Gutiérrez
Methodology: Haifeng Xiao, Alexander Stark, Pedro J. Gutiérrez
Project administration: Luisa M. Lara, Pedro J. Gutiérrez

Abstract Due to its eccentric orbit, Mercury experiences a varying gravitational pull from the Sun along its orbit, leading to periodic surface tidal deformation. The previous measurement of Mercury's tidal h_2 by Bertone et al. (2021, https://doi.org/10.1029/2020je006683) is based on minimizing height differences at cross-overs of the Mercury Laser Altimeter (MLA) profiles. However, this method can suffer from significant interpolation errors. In this study, we apply an alternative approach, which is based on the co-registration of reprocessed MLA profiles. For the reprocessing, we account for the pointing aberration and incorporate an updated spacecraft orbit model. Within the study region of 77°N to 84°N, we obtain a tidal h_2 of 0.92±0.58 (3-σ). This value is compatible with current interior structure and rheology models, but significantly lower than the previous estimate of 1.55±0.65 (3-σ). When combined with recent tidal k_2 estimates, our measurement favors a small to medium-sized inner core.

Plain Language Summary Featuring an eccentricity of ∼0.21, Mercury's orbit is the most elliptical among all the planets in the Solar System. During Mercury's journey around the Sun, the varying gravitational pull periodically stretches and squeezes the planet, leading to observable surface tidal deformation. The magnitude of this deformation depends on Mercury's deep interior, and constraining this quantity can thus shed insights into its interior properties. Bertone et al. (2021, https://doi.org/10.1029/2020je006683) measured Mercury's tidal deformation using height differences at laser tracks' intersection points. However, only the lower bound of their measured magnitude is compatible with the theoretical values from interior modelings. In this study, we reprocess the Mercury Laser Altimeter height profiles, and apply an alternative approach, which is based on the co-registration technique, to look into Mercury's tidal deformation. In principle, we shift the laser profiles in 3-D dimensions so that it can fit with a reference topographic model. We carry out the application at the very north polar region of Mercury. Our measured magnitude is significantly lower than that of Bertone et al. (2021, https://doi.org/10.1029/2020je006683), and is compatible with existing models. Our measurement favors a small to medium-sized solid inner core.

1. Introduction

Mercury is the Sun-scorched innermost planet, an enigmatic world of extremes (Solomon et al., 2018). Understanding the interior structure and core cooling history of the planet can provide critical information on the building blocks that formed the Solar System, especially the terrestrial worlds. Moments of inertia acquired from measuring the libration, obliquity, and its quadrupole gravitational coefficients can be used to constrain the interior of Mercury (e.g., Bertone et al., 2021; Genova et al., 2019, 2021; Hauck et al., 2013; Konopliv et al., 2020; Peale, 1981; Peale et al., 2002; Smith et al., 2012; Stark et al., 2015). Another efficient means to infer knowledge on a planet's interior structure is their tidal response to the gravitational attraction from other objects. While the tidal Love number k_2 describes the secondary potential induced by the internal mass redistribution as a consequence of the external gravitational forcing, the tidal Love number h_2 expresses the corresponding radial surface deformation. Constraining the h_2/k_2 ratio can be used to infer the size of Mercury's solid inner core (Steinbrügge, Padovan, et al., 2018). The eccentricity tides are the largest in each degree since the relative motion of the Sun is approximately in the equatorial plane of Mercury. The largest magnitudes for the tidal distortion coefficients are thus commensurable with the orbital periods of Mercury (see also Stark et al., 2023; Van Hoolst & Jacobs, 2003).

To gain insight into Mercury's interior, the tidal k_2 can be measured by radio science experiments (e.g., Genova et al., 2019; Mazarico, Genova, et al., 2014) while the assessment of the tidal h_2 typically requires laser or radar

Resources: Haifeng Xiao, Alexander Stark, Gregor Steinbrügge, Luisa M. Lara, Pedro J. Gutiérrez
Software: Haifeng Xiao, Alexander Stark
Supervision: Alexander Stark, Luisa M. Lara, Pedro J. Gutiérrez
Validation: Haifeng Xiao, Gregor Steinbrügge, Arthur Briaud, Pedro J. Gutiérrez
Visualization: Haifeng Xiao
Writing – original draft: Haifeng Xiao
Writing – review & editing: Haifeng Xiao, Alexander Stark, Gregor Steinbrügge, Arthur Briaud, Luisa M. Lara, Pedro J. Gutiérrez

altimetry measurements (e.g., Bertone et al., 2021; Steinbrügge, Schroeder, et al., 2018). To date, laser altimetry measurements on Mercury have been obtained by the Mercury Laser Altimeter (MLA) onboard NASA's MErcury Surface, Space ENvironment, GEochemistry and Ranging (MESSENGER, Cavanaugh et al., 2007), which explored the planet in orbit from March 2011 to April 2015. With a sampling rate of 8 Hz, MLA obtained a total of 3,270 profiles containing more than 22 million footprints during the 4 years of orbital phase. The distance between contiguous footprints varies with the velocity of the spacecraft and is between 170 and 440 m. The laser footprint diameters are dependent on the ranging distance and vary between 16 and 134 m. The orbital profiles cluster in the northern hemisphere due to MESSENGER's eccentric, near-polar orbit and the limitation of MLA's maximum ranging distance (∼1,500 km). Constrained by the fact that MESSENGER should always have its sunshade facing the Sun, off-nadir angles generally increase southward and can be as high as 60°. The geolocation accuracy of the footprints mainly depends on the quality of the spacecraft orbit and attitude, laser boresight alignment, and laser shot timing (Xiao et al., 2021). In the case of MLA, it is on the order of ∼10 m (Zuber et al., 2012).

In order to obtain h_2 from laser altimetry, differential height measurement at intersecting points of laser profiles, the so-called cross-overs, are typically used (Bertone et al., 2021; Mazarico, Barker, et al., 2014). However, this method can suffer from significant interpolation errors when the distance between consecutive footprints is large (for MLA, the distance between each cross-over and its bracketing footprints can be 200 m on average), and where the terrain is rough. Furthermore, acute angles between intersecting tracks acquired on a polar orbit around slowly rotating bodies, as is the case with MLA and Mercury, pose an unfavorable geometry for the estimation of cross-over height differences. In this case, even limited cross-track displacements are capable of dramatically shifting the intersection points along the track (Xiao et al., 2021). By minimizing height differences at MLA cross-overs, Bertone et al. (2021) obtained a tidal h_2 of 1.55±0.65 (3-σ). The range spanned by the error bar is only marginally compatible with current models for the interior structure and rheology of Mercury. As acknowledged by Bertone et al. (2021), only their lower limit is consistent with published models (0.85±0.08 from Steinbrügge, Padovan, et al. (2018) and 1.02±0.12 from Goossens et al. (2022)).

An alternative to the cross-over analysis is based on simultaneous inversion of tidal deformations and local topography parameterized using 2-D cubic B-splines (Koch et al., 2008; Thor et al., 2020). However, this method does not account for the lateral shifts of the profiles and is very sensitive to systematic pointing errors and Cauchy-distributed noise. In addition, the resolution of the splines is insufficient to model the small-scale topographic roughness.

In this study, we reprocess the location of MLA profiles by accounting for a pointing aberration that the archived data set does not include (Xiao et al., 2021) and incorporating an updated orbit model (Andolfo et al., 2024). Based on the reprocessed profiles, we then investigate Mercury's tidal deformation using our co-registration technique. Previously, this technique was successfully applied to the Mars Orbiter Laser Altimeter (MOLA) profiles to obtain the spatio-temporal thickness variations of the seasonal CO_2 snow/ice in the Martian polar regions (Xiao, Stark, Schmidt, et al., 2022). The use of the co-registration technique can naturally compensate for the shifts of the profiles and avoid the interpolation errors appearing in the cross-over analysis. To quantify uncertainty and sensitivity, we generate synthetic observations by adding realistic errors and tidal deformation assuming an a priori tidal h_2. Furthermore, we discuss the implications of our measurement on the properties of the Mercurian core.

2. Methods

2.1. Updated Geolocation of MLA Profiles

The analysis of this study is based on the MLA Reduced Data Record (RDR) MESSMLA2001 data set (Neumann, 2018). Xiao et al. (2021) showed that the archived MLA data set does not consider the pointing aberration due to the relative velocity of MESSENGER with respect to the Solar System Barycenter (SSB), which can be up to 63 km/s. If the pointing aberration is left uncorrected, the error in profile location can be of up to 150 m laterally and up to 50 m radially. In our study, we include the aforementioned correction by adopting the Pointing Aberration Model (PAM) as described in Xiao et al. (2021). At the same time, we incorporate an updated MESSENGER orbit model from Andolfo et al. (2024) which builds on an improved model of non-conservative forces, including thermal reradiation effects. Note that radio-tracking data collected at Sun-Probe-Earth (SPE) angles less than 35°are not included in their analysis, resulting in gaps in MESSENGER's reconstructed trajectory (Text S1 in Supporting Information S1). As for the original MESSMLA2001 data set, we adopt the IAU2015

Mercury rotational model (Archinal et al., 2018) for the computation of body-fixed coordinates of MLA footprints. In order to reduce the impact of noise and false returns, we only use footprints with a quality flag of 0, that is, returns from channel 1 high threshold with the highest signal-to-noise ratio (Text S1 in Supporting Information S1).

2.2. Reference DEM From Self-Registration of the Reprocessed MLA Profiles

First, we derive a reference topographic model that represents the static mean surface and against which measurements of surface height variations are to be made (Text S2 and Figure S1 in Supporting Information S1). To achieve this, a random subset of laser profiles is selected and then co-registered to a Digital Elevation Model (DEM) generated from the remaining profiles (Barker et al., 2020). After repeating this process 25 times, we effectively remove the relative offsets between the profiles (Xiao, Stark, Steinbrügge, et al., 2022). By gridding the point cloud from the self-registered profiles, a self-consistent reference DEM with a grid size of 250 m is obtained. Note that only footprints acquired with an off-nadir angle less than 5°are used in the self-registration process.

2.3. Co-Registration and Post-Correction Procedures to Form Tidal Deformation Time Series

In order to obtain time series of the surface tidal deformation, the following steps are performed. First, we filter out footprints acquired with off-nadir angles larger than 2°from the reprocessed profiles. Then, each of the reprocessed profiles after filtering is co-registered to the reference DEM (Section 2.2), parameterizing in lateral and radial shifts. Hence, we obtain an individual height correction for each of the reprocessed profiles at the corresponding observation epoch. Finally, the tidal deformation time series is obtained by evaluating those height corrections as a function of Mercury's mean anomaly.

To reduce the radial offsets of the profiles due to, among others, remaining errors in spacecraft orbit and attitude, laser alignment, and those induced by clock aging and drift, the *Adjustment using Bounds* (henceforth, AuB) method is introduced. This procedure takes advantage of the fact that the tidal h_2 should fall within 0.5 and 2.5 (Figure S4 in Supporting Information S1). All existing observations and modelings yield a tidal h_2 that is greater than 0.5 (e.g., Bertone et al., 2021; Goossens et al., 2022; Steinbrügge, Padovan, et al., 2018; Van Hoolst & Jacobs, 2003). The maximum deformation bound can be placed by assuming the homogeneous fluid limit where the tidal h_2 equals 2.5. The first step of AuB is to locate temporally close pairs of height corrections falling beyond the two ends of the expected tidal deformation range. Then, opposite height adjustments with the same magnitude are applied to bring each of these height correction pairs as close as possible to the reasonable tidal deformation range. In this way, no temporal bias is introduced. We set a temporal separation threshold of 2° in terms of Mercury's mean anomaly, that is, half a day on average. We iterate this search and adjustment process five times when no further adjustments are applicable. The remaining clusters of height corrections falling 2 m away from the expected tidal deformation range are considered erroneous returns and are therefore filtered out.

It should be noted that the tidal response depends on the period of the tidal forcing. For example, the planetary body can react as a fluid when subjected to the static component of the tidal potential. Thus, we exclude the static component of the tidal potential from our analysis. The static component of the tidal potential can be represented and removed by examining the degree-2 spherical harmonic coefficients that remain invariable with time (Stark et al., 2023). For the dynamic tidal potential and the resultant periodic tidal deformation, we focus on the main component that follows the orbital period of 87.97 days. Furthermore, we assume that the tidal response is fully elastic with no phase lag of the tidal bulge and hence no viscoelastic dissipation. This is justified by the fact that the theoretical tidal phase lag should not exceed 4° (Steinbrügge, Padovan, et al., 2018).

In addition to AuB, we implement the *Regional Pseudo Cross-over Adjustment* (henceforth, RPCA) to refine the height corrections obtained. This allows us to improve the precision of the obtained surface tidal deformation time series and, therefore, that of the inverted tidal h_2 (Xiao, Stark, Steinbrügge, et al., 2022). The principle is to make constant height adjustments for each of the profiles. This aims to minimize the height misfits at the pseudo cross-overs where negligible tidal deformation is expected. The height misfit at a pseudo cross-over is assigned as the difference in height corrections in the co-registration of the profile pair, that forms the pseudo cross-over, to the underlying MLA reference DEM (Figure S5 in Supporting Information S1). With this practice, the disadvantages of using height differences at cross-overs can be largely avoided, especially the impact of interpolation errors. In addition, since the profile pair forming a pseudo cross-over does not necessarily intersect, the available number of

pseudo cross-overs can be significantly increased. At the same time, the profile pairs forming the pseudo cross-overs can be widely distributed across the region of interest, the offered constraints are thus more global.

Height misfits at pseudo cross-overs with an expected surface tidal deformation difference less than 8 cm between the two profiles that form them are minimized in the RPCA. The a priori h_2 of 1 is assumed to calculate the tidal deformation sampled by the profiles when executing the selection criterion. Systematic errors with periods that do not match the tidal period are expected to average out. Height differences at pseudo cross-overs are also weighted (Text S3 in Supporting Information S1). Ridge regression is introduced to stabilize the ill-posed least-squares problem due to limited geometric constraints on the model parameters. The ridge trace is implemented to locate the optimal regularization strength. The tidal h_2 can then be inverted by comparing the dynamic tidal potential at the sampling locations of each profile and the obtained tidal deformation.

2.4. Simulations for Verification of the Approach and Uncertainty Quantification

We simulate MLA profiles by making use of the high-resolution surface reference DEM from the self-registration of the reprocessed MLA profiles (Section 2.2). First, we assign the reference DEM heights to the reprocessed profiles at their locations before the co-registration. Then, we add realistic lateral and radial shifts to these synthetic profiles. These shifts are obtained by co-registering the reprocessed MLA profiles to the self-registered reference DEM (Section 2.3). Then, we shuffle these lateral and radial shifts and add them to the synthetic profiles. In this way, the real, not perfectly Gaussian, distributions of these shifts are preserved. No linear drifts are added due to relatively short length of the profiles (Section 3). In addition, height misfits at individual footprint of a randomly chosen profile after its co-registration are sampled following their order along the profile and added to the synthetic profiles. Thus, the realistic distribution of these height misfits and their along-track autocorrelation are preserved. These height misfits can represent the smaller scale topography captured by the MLA footprint (mostly tens of meters in diameter) but not by the reference DEM (250 m/pix), and radial errors induced by pointing jitter among others. Thus, these simulations should contain all error sources. Lastly, we add to these synthetic profiles a prefixed degree-2 dynamic tidal deformation in height using various a priori tidal h_2 values.

Once we have these synthetic profiles, the approach described in Section 2.3 is applied to obtain the tidal deformation as a function of Mercury's mean anomaly, from which the tidal h_2 can then be inverted and compared with the truth.

2.5. Application to the Reprocessed MLA Profiles

After verification and error quantification of the proposed approach by using the simulations described in Section 2.4, we apply it to the actual reprocessed profiles to obtain the surface height variations due to the solid-body tide. The tidal h_2 is then inverted and corrected for any bias induced by the approach. Again, only the dynamic component of the tidal potential is used to invert the tidal h_2 of Mercury.

3. Study Area

We focus on the ring area from 77°N to 84°N in the very north polar region where the laser footprints are the densest. The research region and the slope distribution within it are shown in Figure S1 in Supporting Information S1. The limited off-nadir pointing angles of the profiles acquired within the study region make these profiles less prone to various error sources. Although the maximum tidal deformation occurs at the equator and its surroundings, our study area is where the zonal tide is the largest (up to 60 cm when assuming a tidal h_2 of 0.85; Hussmann & Stark, 2020).

4. Results

Here, we first show the initial height corrections obtained from co-registering the actual profiles to the generated reference DEM. Then, we present a set of simulations to examine the expected performance of our approach. Finally, we show the application to the actual profiles and our estimate of the tidal h_2.

Originally, 9,894,290 footprints from 3,155 profiles are available from the MESSMLA2001 data set. The number of footprints drastically reduces to 3,249,030 after the filtering. Then, 2,107,685 from 1,607 profiles remain after the reprocessing. Finally, after the self-registration, these values stand at 1,931,971 footprints from 1,183 profiles. The remaining measurements feature the best self-consistency, which are then used to generate the reference

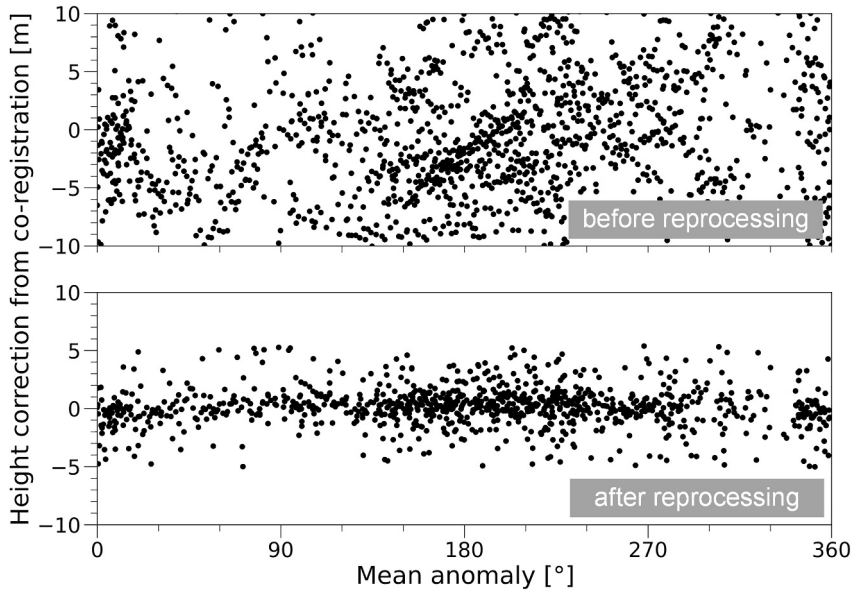

Figure 1. Height corrections from co-registration of the MLA profiles before (top panel) and after (bottom panel) the reprocessing to the reference DEM, plotted as a function of Mercury's mean anomaly. Each dot denotes one height correction obtained from a specific profile. Note that the sign of the height corrections is reversed in order to represent the trend of the tidal deformation.

DEM (Text S1 in Supporting Information S1). Before the reprocessing, height corrections from the successful co-registration of a total of 1,844 profiles to the reference DEM can be up to more than 10 m, and there are no sensible patterns visible (top panel in Figure 1). After the reprocessing, the height corrections of a total of 1,170 profiles have been significantly reduced with a standard deviation of 1.6 m (bottom panel in Figure 1). A general trend of the curve reaching a maximum when Mercury is at aphelion is revealed, and resembles that of the dynamic tidal deformation (gray lines in Figure 3). This shows that reprocessing can significantly facilitate the extraction of the tidal signal.

For the simulations, we study four a priori h_2 values of 0.5, 1, 1.5 and 2, and carry out a total of 50 runs for each case. This is the minimum number needed to stabilize the statistics. The lateral shifts added to the synthetic profiles have a mean of 108 m with a standard deviation of 71 m. The radial shifts added are those shown in the bottom panel of Figure 1. The optimal regularization adopted for each of the four cases is 8, 10, 10, and 15, respectively. An example of the height corrections obtained, before and after the post-corrections, can be seen in Figures S6–S8 in Supporting Information S1, respectively. The inverted tidal h_2 values and their comparison with the truth are shown in Figure 2. The mean and standard deviations of the inverted h_2 for each a priori h_2 are depicted in the error bars. The standard deviation is around 0.1 for all four sampled a priori h_2 values. The bounds representing the three standard deviations can completely entail all the simulation values and thus can be treated as the upper limit in our uncertainties. From the plot, it is evident that the procedures employed induce a systematic bias in the retrieved h_2 estimates. We linearly fit the means of the inversions ($y = 0.62x + 0.28$) to be better compared to the truth ($y = x$). For the a priori h_2 of 0.5, there exists an overestimation on the order of 0.1. In contrast, for the a priori h_2 of 1, 1.5, and 2, there exists quasi-linearly increasing underestimation which can range from 0.1 to 0.5. This is due to the fact that RPCA tends to over-smooth the arching dome of the tidal deformation (Figure S8 in Supporting Information S1). The over-smoothing becomes more effective for a higher tidal h_2, when the dome is more obvious. Furthermore, the lower bound within the AuB procedure, by assuming a tidal h_2 of 0.5, may cause the overestimation intrinsic to our approach when the a priori h_2 is smaller than ∼0.75. These induced biases require correction when evaluating the estimated h_2 from the actual profiles.

After demonstrating the feasibility of the proposed method using the synthetic profiles, we apply the approach to the actual MLA reprocessed profiles. The initial height corrections and those after the AuB adjustment are shown in Figure 1; Figure S9 in Supporting Information S1, respectively. For the RPCA post-correction, a total of 246,202 pseudo cross-overs are available. The obtained tidal deformation curve starts to stabilize when the

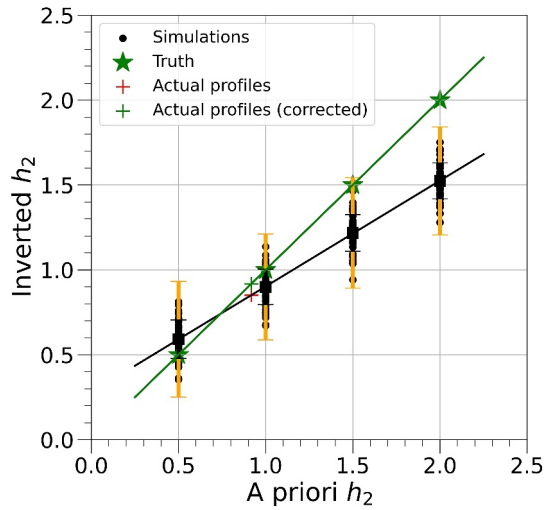

Figure 2. Simulation results as compared to truth for different a priori h_2 values. Black dots represent the tidal h_2 inversions from individual simulations. Statistics of the black dots represented by each error bar are mean, one (in black) and three (in orange) standard deviations. The four mean values from the simulations roughly scale linearly with the truth (black line). This allows us to define a correction as function of the retrieved h_2. Red cross represents the tidal h_2 from the actual reprocessed profiles and the green one denotes its corresponding value after being corrected for the induced underestimation.

regularization is greater than 5, and here we adopt the optimal strength of 10. The final tidal deformation time series is shown in Figure 3. The inverted tidal h_2 is 0.851 with a formal error of 0.01, as represented by the red cross in Figure 2. Considering the bias introduced by our procedures, as described above, this retrieved value needs to be corrected. From our simulations, the retrieved h_2 can be underestimated by 0.07 in magnitude and would give a final tidal h_2 of 0.92 (green cross in Figure 2). In terms of uncertainty, the standard deviation of the simulations at the a priori h_2 of 1 is considered, that is, 0.10. After accounting for the ratio between the inverted h_2 from the simulations and the truth (the slope of the black line in Figure 2), the standard deviation then scales to 0.16. In addition, the formal error of the tidal h_2 inversion, the measurement errors of the individual height corrections (Text S4 in Supporting Information S1), and the sensitivity to different weighting schemes (Text S3 in Supporting Information S1) would further calibrate our measurement to 0.92±0.19 (1-σ) or 0.92±0.58 (3-σ). It should be noted that our estimate is robust against various existing rotation models (Text S5 in Supporting Information S1). We also perform parametric experiments in which 75% of the reprocessed profiles are randomly selected and used for measurement. We complete 50 runs and obtain a mean of 0.849 with a standard deviation of 0.002, which can be neglected. In this study, the co-registration of the profiles is carried out over Mercury's surface, while Bertone et al. (2021) directly applied corrections to the orbits. However, non-linearity between offsets of the ground tracks and those of the orbits is unlikely to bias our measurement (Text S6 in Supporting Information S1). We note that the 3-D shifts added in generating the synthetic profiles already contain height variations due to the body tides and errors associated with the co-registration process. Hence, the cited uncertainties stand at the conservative ends.

5. Discussion

5.1. Possible Local Tidal Deformation Patterns

Our retrieved value of $h_2 = 0.92 \pm 0.19$ is consistent at 1-σ level with the ranges predicted by Steinbrügge, Padovan, et al. (2018); Steinbrügge et al. (2021) and by Goossens et al. (2022), situating the central value on the upper end of the former models, and on the lower end of the latter models. This can be seen in Figure 4. It should be noted that the tidal deformation that we obtain is only representative of the study region, which is at the very north polar region of Mercury. In contrast, Bertone et al. (2021) have adopted all MLA profiles in their analysis which cover the entire northern hemisphere. We have tried to do the same at lower latitudes from 70°N to 77°N where the density of the footprints is still relatively high. Unfortunately, we cannot obtain a reliable tidal h_2 at lower latitudes and determine if there exist pronounced spatially varying patterns of the solid-body tidal deformation, although it is unexpected (e.g., Rovira-Navarro et al., 2024). The measurement of Mercury's tidal deformation is listed as one of the main objectives of the BepiColombo Laser Altimeter (BELA) onboard the Mercury Planetary Orbiter (MPO) spacecraft (Thomas et al., 2021). The instrument's enhanced geolocation performance and global coverage mean that we can quantify and compare Mercury's tidal response at both its north and south polar regions. If we obtain a distinctly incompatible tidal deformation signal, then higher degree/order tidal potential needs to be examined. Or when these measurements cannot be well captured by the current tidal model, that is, the Love number formalism, then we need to think beyond and new models will have to be devised (e.g., Dmitrovskii et al., 2022; Rovira-Navarro et al., 2024).

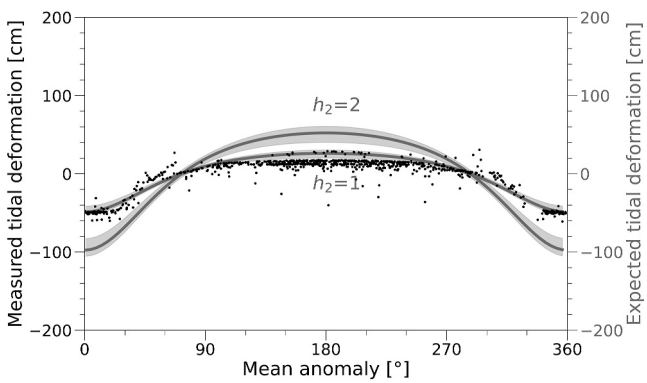

Figure 3. Height corrections from the bottom panel of Figure 1 after the post-corrections. Gray lines represent the average theoretical dynamic tidal deformation with an assumed tidal h_2 of 1 and 2, respectively. Gray shades denote the corresponding expected range of tidal deformation over the study area. Note that the unit is centimeter. Over-smoothing of the arched dome from mean anomaly 90° to 270° is visible.

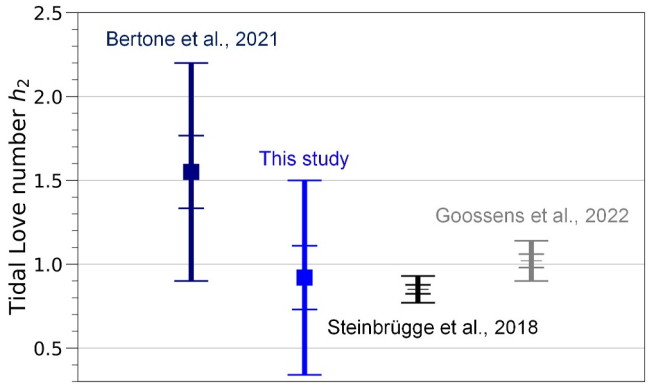

Figure 4. Comparison of our measured tidal h_2 to existing observation and modeling values. Error bars mark the 1-σ and 3-σ bounds, respectively.

5.2. Implications for Mercury's Core

Similar to the tidal Love number k_2, h_2 serves as evidence of the presence of an extended liquid core. Therefore, the h_2 value presented here adds another layer of evidence to this peculiarity of Mercury's interior structure. Moreover, the magnitude of h_2 depends on the rheology of the mantle. While earlier measurement of $k_2 = 0.451 \pm 0.014$ (Mazarico, Genova, et al., 2014) suggested a very cold and stiff silicate mantle (Padovan et al., 2014), the most recent results by Genova et al. (2019, 0.569±0.025) and Konopliv et al. (2020, 0.53±0.03) have revised this view in favor of a less rigid mantle. The ratio of h_2/k_2 can also be diagnostic of the inner core size, particularly if the inner core is large (Steinbrügge, Padovan, et al., 2018). For small and medium inner cores, this ratio would be around 1.75. The central value of $h_2 = 0.92$ would fall very close to this value when combined with the k_2 measured by Konopliv et al. (2020) and slightly below it when combined with the k_2 measured by Genova et al. (2019). However, given the uncertainties in these measurements, no additional constraints can be provided on the inner core size.

6. Conclusion

Among the various geodetic parameters, solid-body tides are of crucial importance for inference about the internal structure of celestial bodies, especially their deep interiors. In this study, we investigate Mercury's tidal deformation by applying a new co-registration technique, complemented with post-correction procedures, to reprocessed MLA profiles. We carry out our study at the very polar region of 77°N to 84°N. For the reprocessing, we include a pointing aberration correction due to relativistic effects and incorporate an updated MESSENGER orbit that has better modeled the non-gravitational forces acting on the spacecraft. We generate realistic synthetic profiles for simulation purposes and show the feasibility of the proposed approach. After that, we apply the validated approach to the reprocessed profiles. We obtain a tidal h_2 of 0.92±0.58 (3-σ). The value of 1.55±0.65 from Bertone et al. (2021) is 68% larger than ours, although both are compatible at 3-σ level. However, our value is compatible with existing theoretical modelings at the 1-σ level. Combined with recent tidal k_2 measurements, our measured tidal h_2 favors a small to medium-sized solid inner core. Further improvement can be expected from data acquired by the BELA instrument onboard BepiColombo (ESA/JAXA), which will begin operations in 2027. In preparation for that, we plan to apply our proposed approach to synthetic BELA profiles to evaluate its capability in obtaining reliable tidal deformation time series, its tidal phase lag, and in disentangling different components of the tides, for example, those with periods of 87.97 and 43.98 days (Stark et al., 2023).

Conflict of Interest

The authors declare no conflicts of interest relevant to this study.

Data Availability Statement

The MESSMLA2001 data set are available for downloading at NASA Planetary Data System (PDS; Neumann, 2018). The reconstructed MESSENGER's trajectories used for the reprocessing of the MLA profiles are archived at SapienzaDataverse (Andolfo, 2024). The MESSENGER attitude, reference frame, and other information needed in the reprocessing are available on the Navigation and Ancillary Information Facility (NAIF, https://naif.jpl.nasa.gov/pub/naif/pds/data/mess-e_v_h-spice-6-v1.0/messsp_1000/data/). Reprocessed profiles and the reference DEM are published in Mendeley Data (Xiao et al., 2024).

Acknowledgments
The authors would like to thank Stefano Bertone (University of Maryland/NASA GSFC), Simone Andolfo and Antonio Genova (University of Rome "La Sapienza") for helpful discussions. The authors acknowledge the MLA team for the data set that enables this research. We also thank Kevin Lewis for handling the manuscript and two anonymous reviewers for constructive comments which helped to significantly improve the manuscript. HX, LML, and PJG acknowledge financial support from project PID2021-126365NB-C21 (MCI/AEI/FEDER, UE) and from the Severo Ochoa Grant CEX2021-001131-S funded by MICIU/AEI/10.13039/501100011033. Part of this research was carried out at the Jet Propulsion Laboratory, California Institute of Technology, under a contract with the National Aeronautics and Space Administration (80NM0018D0004). AB is supported by the German Science Foundation (DFG) project OB 124/29-1.

References

Andolfo, S. (2024). Reconstructed trajectories of the MESSENGER spacecraft [Dataset]. *SapienzaDataverse*. https://doi.org/10.13133/UNIROMA1/A1RMX1

Andolfo, S., Genova, A., & Del Vecchio, E. (2024). Precise orbit determination of MESSENGER spacecraft. *Journal of Guidance, Control, and Dynamics*, 1–13. https://doi.org/10.2514/1.G007690

Archinal, B. A., Acton, C. H., A'Hearn, M. F., Conrad, A., Consolmagno, G. J., Duxbury, T., et al. (2018). Report of the IAU working group on cartographic coordinates and rotational elements: 2015. *Celestial Mechanics and Dynamical Astronomy*, *130*(3), 22. https://doi.org/10.1007/s10569-017-9805-5

Barker, M. K., Mazarico, E., Neumann, G. A., Smith, D. E., Zuber, M. T., & Head, J. W. (2020). Improved LOLA elevation maps for South Pole landing sites: Error estimates and their impact on illumination conditions. *Planetary and Space Science*, *203*, 105–119. https://doi.org/10.1016/j.pss.2020.105119

Bertone, S., Mazarico, E., Barker, M., Goossens, S., Sabaka, T., Neumann, G., & Smith, D. E. (2021). Deriving Mercury geodetic parameters with altimetric crossovers from the Mercury Laser Altimeter (MLA). *Journal of Geophysical Research: Planets*, *126*(4), e2020JE006683. https://doi.org/10.1029/2020JE006683

Cavanaugh, J. F., Smith, J. C., Sun, X., Bartels, A. E., Ramos-Izquierdo, L., Krebs, D. J., et al. (2007). The Mercury Laser Altimeter instrument for the MESSENGER mission. *Space Science Reviews*, *131*(1), 451–479. https://doi.org/10.1007/s11214-007-9273-4

Dmitrovskii, A. A., Khan, A., Boehm, C., Bagheri, A., & van Driel, M. (2022). Constraints on the interior structure of Phobos from tidal deformation modeling. *Icarus*, *372*, 114714. https://doi.org/10.1016/j.icarus.2021.114714

Genova, A., Goossens, S., Mazarico, E., Lemoine, F. G., Neumann, G. A., Kuang, W., et al. (2019). Geodetic evidence that Mercury has a solid inner core. *Geophysical Research Letters*, *46*(7), 3625–3633. https://doi.org/10.1029/2018GL081135

Genova, A., Hussmann, H., Hoolst, T. V., Heyner, D., Iess, L., Santoli, F., et al. (2021). Geodesy, geophysics and fundamental physics investigations of the BepiColombo mission. *Space Science Reviews*, *217*(2), 31. https://doi.org/10.1007/s11214-021-00808-9

Goossens, S., Renaud, J. P., Henning, W. G., Mazarico, E., Bertone, S., & Genova, A. (2022). Evaluation of recent measurements of Mercury's moments of inertia and tides using a comprehensive Markov Chain Monte Carlo method. *The Planetary Science Journal*, *3*(2), 37. https://doi.org/10.3847/PSJ/ac4bb8

Hauck, S. A., Margot, J. L., Solomon, S. C., Phillips, R. J., Johnson, C. L., Lemoine, F. G., et al. (2013). The curious case of Mercury's internal structure. *Journal of Geophysical Research: Planets*, *118*(6), 1204–1220. https://doi.org/10.1002/jgre.20091

Hussmann, H., & Stark, A. (2020). Geodesy and geophysics of Mercury: Prospects in view of the BepiColombo mission. *The European Physical Journal Special Topics*, *229*(8), 1379–1389. https://doi.org/10.1140/epjst/e2020-900211-4

Koch, C., Christensen, U., & Kallenbach, R. (2008). Simultaneous determination of global topography, tidal Love number and libration amplitude of Mercury by laser altimetry. *Planetary and Space Science*, *56*(9), 1226–1237. https://doi.org/10.1016/j.pss.2008.04.002

Konopliv, A., Park, R., & Ermakov, A. (2020). The Mercury gravity field, orientation, love number, and ephemeris from the MESSENGER radiometric tracking data. *Icarus*, *335*, 113386. https://doi.org/10.1016/j.icarus.2019.07.020

Mazarico, E., Barker, M. K., Neumann, G. A., Zuber, M. T., & Smith, D. E. (2014). Detection of the lunar body tide by the Lunar Orbiter Laser Altimeter. *Geophysical Research Letters*, *41*(7), 2282–2288. https://doi.org/10.1002/2013GL059085

Mazarico, E., Genova, A., Goossens, S., Lemoine, F. G., Neumann, G. A., Zuber, M. T., et al. (2014). The gravity field, orientation, and ephemeris of Mercury from MESSENGER observations after three years in orbit. *Journal of Geophysical Research: Planets*, *119*(12), 2417–2436. https://doi.org/10.1002/2014JE004675

Neumann, G. (2018). MESSENGER MLA calibrated (CDR/RDR) data bundle [Dataset]. *NASA Planetary Data System*. https://doi.org/10.17189/1518580

Padovan, S., Margot, J.-L., Hauck, S. A., Moore, W. B., & Solomon, S. C. (2014). The tides of Mercury and possible implications for its interior structure. *Journal of Geophysical Research: Planets*, *119*(4), 850–866. https://doi.org/10.1002/2013JE004459

Peale, S. J. (1981). Measurement accuracies required for the determination of a Mercurian liquid core. *Icarus*, *48*(1), 143–145. https://doi.org/10.1016/0019-1035(81)90160-3

Peale, S. J., Phillips, R. J., Solomon, S. C., Smith, D. E., & Zuber, M. T. (2002). A procedure for determining the nature of Mercury's core. *Meteoritics & Planetary Science*, *37*(9), 1269–1283. https://doi.org/10.1111/j.1945-5100.2002.tb00895.x

Rovira-Navarro, M., Matsuyama, I., & Berne, A. (2024). A spectral method to compute the tides of laterally-heterogeneous bodies. *The Planetary Science Journal*, *5*(5), 129. https://doi.org/10.3847/PSJ/ad381f

Smith, D. E., Zuber, M. T., Phillips, R. J., Solomon, S. C., Hauck, S. A., Lemoine, F. G., et al. (2012). Gravity field and internal structure of Mercury from MESSENGER. *Science*, *336*(6078), 214–217. https://doi.org/10.1126/science.1218809

Solomon, S. C., Nittler, L. R., & Anderson, B. J. (2018). *Mercury: The view after MESSENGER* (Vol. 21). Cambridge University Press. https://doi.org/10.1017/9781316650684

Stark, A., Hussmann, H., Fienga, A., Hu, X., Oberst, J., Rambaux, N., et al. (2023). Frequency-dependent viscoelastic tides of Mercury. *Lunar and Planetary Science Conference*, *2806*, 2889.

Stark, A., Oberst, J., Preusker, F., Peale, S. J., Margot, J.-L., Phillips, R. J., et al. (2015). First MESSENGER orbital observations of Mercury's librations. *Geophysical Research Letters*, *42*(19), 7881–7889. https://doi.org/10.1002/2015GL065152

Steinbrügge, G., Dumberry, M., Rivoldini, A., Schubert, G., Cao, H., Schroeder, D. M., & Soderlund, K. M. (2021). Challenges on Mercury's interior structure posed by the new measurements of its obliquity and tides. *Geophysical Research Letters*, *48*(3), e2020GL089895. https://doi.org/10.1029/2020GL089895

Steinbrügge, G., Padovan, S., Hussmann, H., Steinke, T., Stark, A., & Oberst, J. (2018). Viscoelastic tides of Mercury and the determination of its inner core size. *Journal of Geophysical Research: Planets*, *123*(10), 2760–2772. https://doi.org/10.1029/2018JE005569

Steinbrügge, G., Schroeder, D. M., Haynes, M. S., Hussmann, H., Grima, C., & Blankenship, D. D. (2018). Assessing the potential for measuring Europa's tidal Love number h_2 using radar sounder and topographic imager data. *Earth and Planetary Science Letters*, *482*, 334–341. https://doi.org/10.1016/j.epsl.2017.11.028

Thomas, N., Hussmann, H., Spohn, T., Lara, L., Christensen, U., Affolter, M., et al. (2021). The BepiColombo Laser Altimeter. *Space Science Reviews*, *217*(1), 1–62. https://doi.org/10.1016/j.pss.2007.03.003

Thor, R. N., Kallenbach, R., Christensen, U. R., Stark, A., Steinbrügge, G., Di Ruscio, A., et al. (2020). Prospects for measuring Mercury's tidal Love number h_2 with the BepiColombo Laser Altimeter. *Astronomy & Astrophysics*, *633*, A85. https://doi.org/10.1051/0004-6361/201936517

Van Hoolst, T., & Jacobs, C. (2003). Mercury's tides and interior structure. *Journal of Geophysical Research*, *108*(E11). https://doi.org/10.1029/2003JE002126

Xiao, H., Stark, A., Schmidt, F., Hao, J., Steinbrügge, G., Wagner, N. L., et al. (2022). Spatio-temporal level variations of the Martian Seasonal North Polar Cap from co-registration of MOLA profiles. *Journal of Geophysical Research: Planets*, *127*(10), e2021JE007158. https://doi.org/10.1029/2021JE007158

Xiao, H., Stark, A., Steinbrügge, G., Briaud, A., Lara, L., & Gutierrez, P. (2024). Reprocessed Mercury Laser Altimeter (MLA) profiles and a Digital Elevation Model (DEM) [Dataset]. *Mendeley Data*. https://doi.org/10.17632/dpyzwbws6k.2

Xiao, H., Stark, A., Steinbrügge, G., Hussmann, H., & Oberst, J. (2021). Processing of laser altimeter Time-of-Flight measurements to geodetic coordinates. *Journal of Geodesy*, *95*(2), 22. https://doi.org/10.1007/s00190-020-01467-4

Xiao, H., Stark, A., Steinbrügge, G., Thor, R., Schmidt, F., & Oberst, J. (2022). Prospects for mapping temporal height variations of the seasonal CO_2 snow/ice caps at the Martian poles by co-registration of MOLA Profiles. *Planetary and Space Science*, *214C*, 105446. https://doi.org/10.1016/j.pss.2022.105446

Zuber, M., Smith, D. E., Phillips, R., Solomon, S., Neumann, G., Ii, S. A. H., et al. (2012). Topography of the northern hemisphere of Mercury from MESSENGER laser altimetry. *Science*, *336*(6078), 217–220. https://doi.org/10.1126/science.1218805